ACS OMEGA

http://pubs.acs.org/journal/acsodf

Article

Anomalous Enrichment of As and Hg in Underground Coal Dust: A Case from Xishan Coalfield, Shanxi Province, North China

Chuange Wang,* Fangui Zeng, Chengxiang Xu, and Qiuyue Xu

Cite This: *ACS Omega* 2023, 8, 13884−13898

Read Online

ACCESS | Metrics & More | Article Recommendations | Supporting Information

ABSTRACT: Coal dust is an important source of coal workers' pneumoconiosis, which is harmful to the health of underground workers. The coal dust samples were directly collected using a coal dust sampler from four major production positions in the underground coal mine. The particle size distribution, mineralogy, and occurrence of As and Hg in the coal dust samples were investigated. The results indicated that the contents of As and Hg were depleted or normal in the parent coal samples compared with the average values of C−P coal in North China and Chinese coal, but they were anomalously enriched in coal dusts. The concentrations of As and Hg in the coal dust samples studied are greater than the values of the elements in the parent coal. The As content in the coal dust samples studied is about one to three orders of magnitude above the parent coal value and the Hg content in the studied coal is 1.28 to 20.28 times higher than the parent coal value. The modes of occurrences of As and Hg were studied by sequential chemical extraction in combination with field emission scanning electron microscopy-energy dispersive spectroscopy (FESEM-EDS) and high-resolution transmission electron microscopy-EDS (HRTEM-EDS). The occurrence of As is dominated mainly by pyrite and secondarily by carbonate and silicate in the coal dust samples. Pyritic Hg and organic Hg may be the dominant forms in mining face and heading face samples, and carbonate and pyritic Hg are the main forms in rocks roadway and return airway samples. It is considered that the mechanochemical effect resulted in the formation of surface active sites and modification of the morphology. Harmful trace elements, such as As, Cd, Hg, Se, Pb, Co, Sb, and Tl, and minor grains associated with nanominerals that bear much hazardous elements, could easily be originally fractionated or adsorbed by airborne particulates. This research aims to provide a theoretical basis for the prevention of occupational disease and underground environmental evaluation.

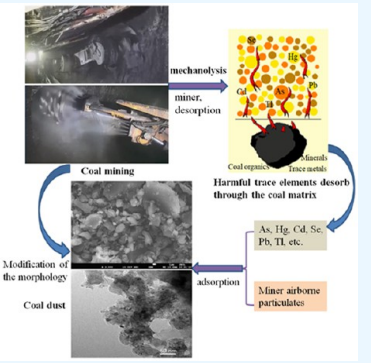

1. INTRODUCTION

For coal miners, the most common and major occupational health hazard is coal mine dust-related respiratory disease. Occupational exposure to coal mine dust will lead to the development of a wide spectrum of pulmonary diseases, such as coal workers' pneumoconiosis (CWP), silicosis, progressive mass fibrosis (PMF), emphysema, chronic bronchitis, and dust-related diffuse fibrosis.[1−4] Investigation of the harmful trace elements in coal mine dust is essential for coal miners' health and its control. Unfortunately, compared with the research on the geochemistry and mineralogy of coal and atmospheric particulate matter, little attention has been paid to coal mine dust, which limits our understanding of its compositions, morphology, and their relation with occupational diseases. Due to its origin from coal and other sedimentary rocks, coal mine dust is a complex mixture containing different proportions of minerals, trace metals, and organics with different grades of coal particulates,[5] especially in underground coal mine. Systematic characterization of the physicochemical properties of nano-sized coal dust must be enforced.

Conventional practice in monitoring and control of respirable coal mine dust has focused on the total mass concentration and the crystalline silica mass fraction of personal exposures.[6−9] SiO_2 can activate gene-cataloging nuclear factors and protein catalysts that induce pneumoconiosis and silicosis.[8,9] Moreover, Harrington et al.[10] found that FeS_2 in coal dust will inflammate the lung cells and produce more reactive oxygen species, which is one of the important factors leading to pneumoconiosis. Stone et al.[11] suggested that the soluble cationic components can conceal the surface activity of quartz. Schulz[12] found that clay minerals are enriched in the lung of miners with severe silicosis and can reduce the cytotoxicity of quartz, and that kaolinite has the potential of self-fibrosis. The composition and distribution of minerals and trace elements and the relationship between them may be more important to the activity of SiO_2.[11,12]

The recent studies concentrated on comprehensively analyzing the particle size distribution, minerals, metals, and toxic trace elements in respirable deposited dust in under-

Received: January 15, 2023
Accepted: March 27, 2023
Published: April 5, 2023

ground coal mines.[13−16] Coal dust from eight mines was collected in five locations: intake airway, feeder, production, roof bolter, and return airway; potentially bioaccessible and total acid-soluble mass concentrations of metals and trace elements were determined using sequential digestions by inductively coupled plasma-mass spectrometry (ICP-MS).[13,14] Su et al.[15] and Trechera et al.[16] collected some deposited dust in coal mines, and systemically analyzed the mineralogy and geochemistry of respirable coal dust. In the process of coal mining, some hazardous elements can enter the atmosphere and be concentrated. As and Hg are divided into senior-grade potentially toxic trace elements that will cause harm or potential harm to the environment and human body with little dose.[17−20] Many researchers have reported the abundance and modes of occurrence of As[21−23] and Hg[23−25] in coals from Chinese coalfields. Results from selective leaching, X-ray absorption fine structure (XAFS), and electron microprobe analysis show that pyrite is the principal source of arsenic in bituminous coal, but the concentration of As in pyrite varies widely; arsenic also appears to be primarily associated with organics, as As^{3+} or arsenate (AsO_4^{3-}).[5] Kolker et al.[26] found that about 75% of the arsenic in bituminous coals was associated with pyrite, while it was only 40% of the arsenic in the low-rank coals. Yudovich et al.[27,28] observed that sulfide sites dominate in high As content, whereas As_{org} dominates in low As content; the As content in silicates is usually minor; both organic and inorganic As can exist in chemically bound form and in sorbed arsenate form. In low-sulfur coals, which are poor in Hg, only two Hg sites dominate: Hg_{org} and $Hg_{sulfide}$; high-sulfur coals usually contain higher amounts of Hg, which occur typically in Hg_{pyr} form. Due to the low abundance and high volatility of As and Hg in coal,[27−29] chemical sequential extraction tests were used to determine their occurrence.[5,21−23,25,26,30]

The systematic study of the mineralogy and geochemical characteristic of coal dust has potentially practical significance and reference value for promoting coal mine safety production and ensuring the health of coal miners. In this paper, underground coal dust was collected directly from the mining face, heading face, rocks roadway, and return airway of No. 2 coal seam in a coal mine of Xishan Coalfield, Shanxi, North China. In addition, the working face coal was gathered and characterized. Particle size distribution was studied using a laser particle size analyzer. The X-ray diffraction technique was used to establish the kinds and relative abundance of the major and minor minerals in the coal dust. Field emission scanning electron microscope-energy dispersive spectroscopy (FESEM-EDS) and high-resolution transmission electron microscopy-EDS (HRTEM-EDS) were performed to observe the morphological features of coal dusts and identify the occurrence of minerals. The harmful trace elements, especially As and Hg, were quantitatively determined by sequential chemical extraction. New findings were discussed to explore the abundance, distribution, and concentration mechanism of As and Hg in underground coal dust due to their anomalous concentration. The research aims to provide a theoretical basis for the prevention of occupational disease and underground environmental evaluation.

2. SAMPLING AND METHODS

2.1. Coal Dust Sample Collection. The coal dusts were collected directly from No. 2 coal seam of a coal mine in Xishan coalfield, Shanxi province, China. The direct roof is medium-grained sandstone, mainly quartz and feldspar, with a thickness of 5.14 m, and the old roof and pseudo-roof are sandy mudstone and mudstone, with thicknesses of 2.78 and 0.3−0.8 m, respectively. The direct bottom is fine-grained sandstone, mainly quartz and feldspar with a thickness of 3.88, and sandy mudstone with a thickness of 0.2 m; the old bottom is sandy mudstone with a thickness of 2.34 m. The sedimentary sequence of the coal content in the strata of Xishan coalfield is presented in Figure 1.

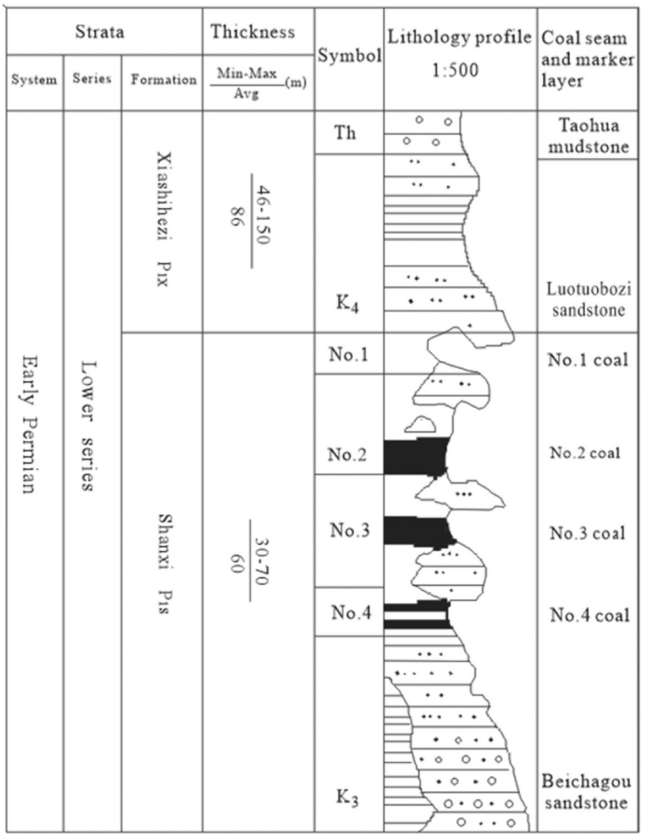

Figure 1. Diagram of the sedimentary sequence of coal content strata of Xishan coalfield, North China.

The mining face is 1535, of which 225 m is in mining. The thickness of No. 2 coal seam is 2.53−3.15 m, the average thickness is 2.89 m, and the mining height is 2.83−3.95 m. The comprehensive mechanized mining method with full height and all collapse in one long wall is adopted. A double drum shearer is used to open the gap, and inclined cutters are fixed at both ends of the mining face. A scraper conveyor is used to transport the coal, and a hydraulic shield support is used to sustain the roof. Coal transportation system is from main roadway along belt to centralized belt roadway, then to centralized coal bunker in mining area, finally transported to ground coal bunker. The mining face is equipped with a main lane and a deputy lane, and U-type ventilation mode is employed. The length of the main lane of the mining face is 58 m. The total air intake is 23,905 m^3/min and the total air return is 24,898 m^3/min. A pure water spray to reduce the dust is applied during mining between the frame and the coal conveying point. The water consumption of the shearer and the transfer point spray is 0.5 m^3/min. The diagram of the roadway layout in the working face of No. 2 coal is shown in Figure 2.

https://doi.org/10.1021/acsomega.3c00300
ACS Omega 2023, 8, 13884−13898

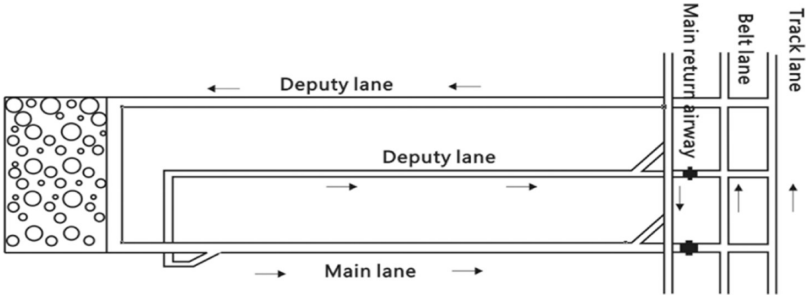

Figure 2. Diagram of the roadway layout in the working face of No. 2 coal.

The coal dust samples were collected from No. 2 coal seam of the underground coal mine in four key locations: fully mechanized mining face, heading face, rocks roadway, and return airway. Sampling was done at the same position over half a month during the fully mechanized coal mining process, and about 20 g of coal dust was collected for each sample. The sampling was conducted using an AKFC-92A mine dust sampler with a nylon Dorr-Oliver cyclone at the flow rate of 10 L/min. The samples were collected directly onto 40 mm polycarbonate filters (PC, track-etched with 0.4 μm pore size). The sampling points of the fully mechanized mining face and heading face were about 10 m away from the mining face, and the sampling height of the rocks tunnel and return airway was about 3 m as observed by a contra-flow collecting method. The samples were collected at the production workplace, and the collection time ranged between 2 and 4 h with the continuous sampling method using several PC filters. The coal dust concentration near different sampling points was found to be 2.6−16.5 mg/m^3, which is far more than the health exposure limit of 0.5−4 mg/m^3 recommended by WHO.[31] The constant total respirable dust concentration was only 1.5 mg/m^3 with static composition, which is the current permissible exposure limit in US underground coal mines.[9,32] In order to compare the mineralogy and elemental composition, the sample of No. 2 parent coal was also collected at the same working face. Ten samples (about 30 kg) were collected along the mining working face and mixed as the parent coal sample.

2.2. Experimental Methodologies. *2.2.1. Petrographic, Ultimate, and Proximate Analyses of No. 2 Parent Coal.* According to GB/T 6948-2008,[33] Zeiss Axioskop 40A Microscope and SP ultraviolet−visible (UV−vis) 4000 microphotometer were used to determine the vitrinite reflectance ($R_{o,max}$, %). The microscopical determination was done under both reflected light and polarized light with oil (N_e = 1.518% at 23 °C, 10×25×). A Zeiss sapphire (R = 0.598%) and yttrium-aluminium-garnet (R = 0.912%) were used as standard. The measured $R_{o,max}$ (%) was 1.96%. The lithotypes of No. 2 coal seam were mainly dominated by clarain and durain, secondarily by vitrain, and lastly by few fusain.

Proximate and ultimate analyses of the coal samples were conducted according to the GB/T 212-2008,[34] GB/T 476-2008,[35] and GB/T 214-2007,[36] separately. The ultimate analyses (C, H, N, S) were performed using a Germany Vario EL III elemental analyzer, and the O content was obtained from the difference. The results of raw coal content are as follows: M_{ad} = 1.04%, A_{ad} = 10.77%, V_{daf} = 14.35%; C_{daf} = 90.40%, H_{daf} = 4.37%, O_{daf} = 2.93%, N_{daf} = 1.52%, $S_{t,\,daf}$ = 0.78%.

2.2.2. Mineralogical and Nanomineralogical Analyses. A particle size distribution test was conducted using a Malvern Mastersizer 2000 laser particle size analyzer. The instrument covers a wide range of particle sizes from 0.02 to 2000 μm, with an accuracy and reproducibility of 1%. Mastersizer 2000 is used to analyze, and draw the frequency and probability cumulative curves. A Bruker D8 Advance X-ray diffractometer was used to determine the mineralogy of the coal dust. The morphology and composition of the organic matter and minerals in the coal dusts were analyzed using JSM-6700F FESEM-EDS and JEM-2100F HRTEM-EDS.

Mineral identifications in the SEM were made on the basis of the morphology and composition of the grains using both secondary electron and backscattered electron modes. The secondary electrons generated in the depth range of 50−500 Å can escape from the surface and be detected because their energy is less than 50 eV. Since the secondary electrons are affected by the surface fluctuation, the morphology of the sample surface can be observed. Because the backscattered electrons are generated at about 5000 Å, the electron beam is scattered, so the resolution of the electron image is not as good as that of the secondary electron image. All work was conducted in a high vacuum at 15 kV, current 600 PA, 12.5 mm working distance, 6.5 μm spot size, 25,000 cps count rate, and 1000×−5000× magnification. The main elemental compositions of nanominerals with unknown phases were determined using EDS. The Fast Fourier Transform (FFT) patterns (lattice distances and angles) of the TEM images were obtained through a digital micrograph (DM) software. Nanominerals always have certain crystal defects (such as additional disordering, shearing, or impurities), which means that there will be slight differences between the tested nanominerals and standard minerals in the Inorganic Compound Powder Diffraction File (PDF) database of Jade 6.5 software.[37]

2.2.3. Sequential Chemical Extraction. The samples were analyzed in parallel; the procedure is as follows: 30 mL of deionized water is added to 2 g of coal dust sample and placed at room temperature in a closed bomb for 24 h. The mixture is centrifuged at a speed of 5000 rpm for 30 min. The residue is washed with water and centrifuged twice. 30 mL of 1 mol/L CH_3COONH_4 is added to the residue in the tricpolypropylene test tube with ultrasonic shaking for 2 h in a water bath at 60 °C. Then, 30 mL of 3 mol/L HCl, HF (48%), and 2 mol/L HNO_3 are added, respectively. Each step is separated by centrifugation at a speed of 5000 rpm for 30 min, and the residues are used for the next step. The supernatants are removed to volumetric flasks and diluted to 50 mL with deionized water for analyses.

The sequence of leaching steps was adopted such that elements associated with various parts of the coal dust would be removed in the following order:[30] (1) exchangeable cations,

https://doi.org/10.1021/acsomega.3c00300
ACS Omega 2023, 8, 13884−13898

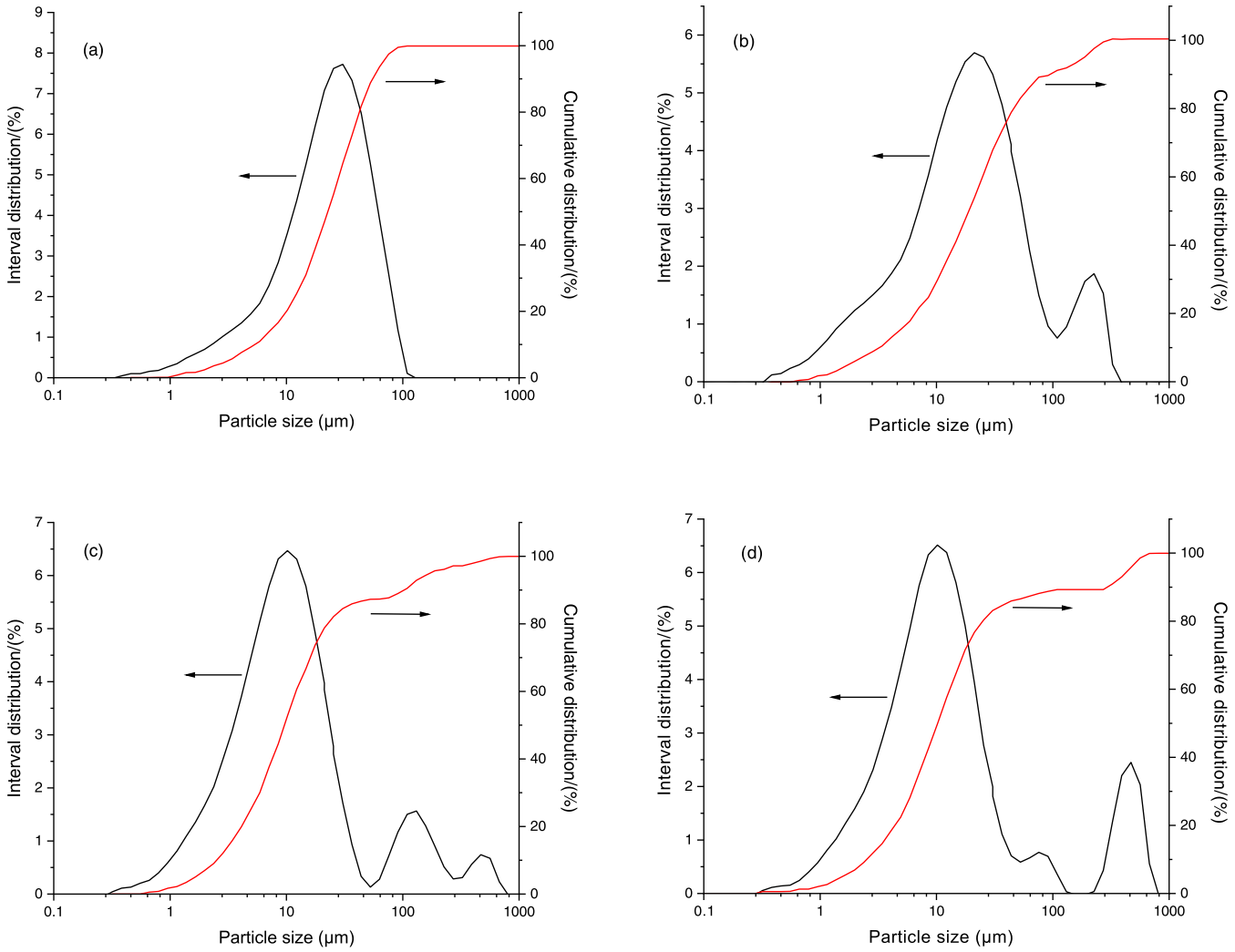

Figure 3. Frequency curve and probability cumulative curve of underground coal mine dust in different locations ((a) mining face, (b) heading face, (c) rocks roadway, and (d) return airway).

and a fraction of the carbonate-hosted cations, are removed by CH_3COONH_4; (2) cations primarily associated with carbonates and monosulfides are removed by HCl; (3) cations associated with silicates (quartz and clays) are removed by HF; and (4) elements associated with disulfides (pyrite and marcasite) are removed by HNO_3. Elements not removed by the leaching process may be present in the organic matrix, or may occur in insoluble phases such as zircon or titanium dioxide.

2.2.4. Determination of Major Elements, As, Hg, and Other Harmful Trace Elements in Coal Dust. According to GB/T 14506.28-2010,[38] the major-element oxides (including SiO_2, Al_2O_3, Fe_2O_3, CaO, Na_2O, K_2O, MgO, MnO, TiO_2, and P_2O_5) in coal dust ash were determined using a PW2404 X-ray fluorescence spectrometer (XRF); the loss on ignition (LOI) was also determined at 815 °C. According to GB/T 14506.12-2010,[39] the F and Cl contents in coal dust were determined using the alkali fusion ion selective electrode method with an AB-104L PHS-25A acidity meter. According to GB/T 14506.30-2010,[40] the harmful trace elements, except As, Hg, F and Cl, were determined using the mixed-acid digestion method by DRC-E inductively coupled plasma-mass spectrometry (ICP-MS). In order to check the accuracy, the slate (OU-6), andesite (AMH-1), and garnet biotite plagioclase gneiss (GBPG-1) were adopted as standard samples, and analytical errors were estimated at about <3%. According to GB/T 22105.2-2008[41] and EJ/T 1149-2001,[42] the contents of As and Hg in raw coal dust and the residue coal dust were determined using an atomic fluorescence spectrometer (AFS) and a DMA80 mercury detector (with a detection limit of 0.005 ng), respectively. According to DZ/T 0064.11-1993,[43] and EPA 7473-2007,[44] As and Hg in the each leaching solutions were determined using AFS and a mercury detector. Data for the raw coal dust were compared with the whole coal dust values to derive the percentages of arsenic and mercury leached by each solvents. Comparison of the solutions and solid residue values allows do mass-balance calculations that providing an internal check on the results, and the extraction yields also can be calculated.

3. RESULTS AND DISCUSSION

3.1. Particle Size Distribution Characteristics. The coal dust samples are classified into four types based on their cross-sectional diameter, i.e., coarse dust (>40 μm), fine dust (10−40 μm), micro-fine dust (0.25−10 μm), and ultrafine dust (<0.25 μm).[45] The particle size analyzed results are shown in Figure 3, and Tables 2 and 3. It was found that coarse grains accounted for 18, 15.57, 3.58, and 4.1%, fine grains accounted

https://doi.org/10.1021/acsomega.3c00300
ACS Omega 2023, 8, 13884−13898

Table 1. Particle Size Distribution of the Coal Dust Samples (%)[a]

	mining face		heading face		rocks roadway		return airway	
particle size (μm)	Di	Ac	Di	Ac	Di	Ac	Di	Ac
0.5	0.08	0.14	0.15	0.35	0.16	0.53	0.14	0.47
1.0	0.23	0.9	0.50	1.98	0.60	2.37	0.57	2.23
2.5	0.85	4.09	1.25	7.62	1.83	9.94	1.62	9.12
5.0	1.49	10.09	1.92	15.71	3.82	24.58	3.26	21.69
10	3.31	22.25	3.48	29.55	5.80	50.37	5.18	44.24
105	0.02	99.26	0.81	92.92	1.19	90.02	1.5	81.49

[a]Di, differential; Ac, accumulate.

Table 2. Major-Element Oxides, and the A_{ad} Values of Coal Dust and No. 2 Parent Coal (%)

	sample	SiO_2	Al_2O_3	Fe_2O_3	MgO	CaO	Na_2O	K_2O	MnO	TiO_2	P_2O_5	A_{ad}
coal dust	mining face	10.01	5.37	2.22	0.152	0.279	0.016	0.321	0.01	0.283	0.021	19.25
	heading face	11.97	7.6	2.1	0.243	0.511	0.01	0.3	0.015	0.37	0.079	23.63
	rocks roadway	23.65	10.51	2.83	0.393	1.37	0.303	1.18	0.026	0.54	0.215	41.08
	return airway	25.12	11.57	2.23	0.485	1.49	0.157	1.12	0.028	0.512	0.232	43
parent coal	vitrain	2.65	2.16	0.673	0.096	0.126	0.046	0.021	0.008	0.103	0.011	5.91
	clarain	4.17	3.19	0.241	0.119	0.18	<0.010	0.012	0.006	0.237	0.011	8.28
	durain	5.31	3.77	0.161	0.079	0.104	0.052	0.028	0.005	0.365	0.013	10
	fusain	33.34	29.32	0.28	0.103	0.479	0.387	0.058	<0.004	0.057	0.05	64.15
	raw coal	5.51	4.22	0.383	0.072	0.224	0.092	0.028	<0.004	0.206	0.01	10.77
AM	CC[17]	8.47	5.98	4.85	0.22	1.23	0.16	0.19	0.015	0.33	0.092	21.54

for 59.01, 47.8, 36.07, and 33.15%, micro-fine grains accounted for 22.25, 29.55, 50.37, and 44.24%, respectively, and ultrafine dust in the samples was low. The particle size ranges of the four coal dust samples are 0.42−115.3, 0.32−316.5, 0.27−691.9, and 0.28−709.6 μm, with the high peak appearing at 28.09, 22.38, 9.73, and 10.24 μm, respectively (Figure 3a−d). The shapes of the frequency curve peak indicate the different sources of airborne dusts.

Respirable coal dust particle size covers a wide range from 1 nm to 10 μm. Particle sizes larger than 10 μm will be blocked by human vibrissa, and those within 5−10 μm will be blocked by the respiratory tract, while particle sizes smaller than 2.5 μm can enter the human lungs.[46] The proportions of $PM_{2.5}$ are 4.09, 7.62, 9.94, and 9.12%, PM_5 are 10.09, 15.71, 24.58, and 21.69%, PM_{10} are 22.25, 29.55, 50.37, and 44.24%, PM_{10-5} are 54.65, 46.84, 51.20, and 50.97%, and $PM_{2.5}$ are 18.38, 25.79, 19.73, and 20.61% for mining face, heading face, rocks roadway, and return airway samples, respectively. The D_{10} sizes of the four coal dust samples are 5.35, 3.18, 2.52, and 2.69 μm, the D_{50} sizes are 23.50, 18.68, 9.91, and 11.64 μm, and the D_{90} sizes are 56.88, 72.40, 104.31, and 304.40 μm, respectively. The specific surface areas are 0.55, 0.79, 1.08, and 0.97 m^2/g, average particle sizes of surface area D[3,2] are 10.92, 7.62, 5.57, and 6.20 μm, and volume average particle diameters D[4,3] are 27.88, 34.88, 37.32, and 71.52 μm, respectively (Table 1).

3.2. Mineralogy of the Coal Dust. The major elements of the coal dusts are dominated by SiO_2, Al_2O_3, and Fe_2O_3 (Table 2). The ash contents on the air dried basis (A_{ad}) of mining face, heading face, rocks roadway, and return airway samples are 19.25, 23.63, 41.08, and 43%, respectively, which are higher than those of vitrain, durain, and clarain (≤10%), and much lower than that of fusain. The ash contents of rocks roadway and return airway samples are more higher than those of raw coal and Chinese coal. Jade 6.5 was used to retrieve the mineral types from the X-ray diffraction (XRD) spectra (Figure 4). The relative contents of the main minerals were determined by semiquantitative methods, and the results are listed in Table 3. This indicated that kaolinite, quartz, pyrite, illite, and siderite were dominated in the coal dust samples, and gypsum and calcite could also be found in them. Kaolinite, quartz, gypsum, and siderite were enriched in the coal lithotypes, especially in fusain. The mineral composition results are consistent with the ash analyses. Minerals, especially quartz and pyrite, were enriched in the coal dust samples, which indicated that the minerals are concentrated in the particulate matters during coal mining.

The scanning electron microscope observation show that all samples contain organic matters and minerals. The minerals in the coal dust samples can be validated by SEM in conjunction with EDS analysis (Figures S1a−i). In comparison with the SEM image in secondary electron mode, organic matters and minerals can easily be distinguished by the colors in backscattered electron mode (Figures S2a−e, and 5). It can be found that the organic matters are abundant in the mining face and heading face samples, which are consistent with the weight loss (Table 2) and XRD test results (Table 3). In addition, underground coal dusts capture many fine particles on the surface, which are quite different from the morphology characteristics of the parent coal dust produced by manual grinding (≤75 μm) (Figure S2e).The morphology and types of minerals can also be comprehensively observed in the FESEM-EDS and HRTEM-EDS images. Kaolinite is generally leaf-shaped (Figure 5a), while quartz has an uneven surface and many intergranular pores (Figure 5b). Octahedral pyrite crystallites are 3−10 μm in size in the heading face coal dust (Figure 5c). Several pyrite particles with diameters of about 1 μm can be seen in the coal organic matter particles (Figure 5d), and cubic pyrite 1.5 × 2.5 μm^2 in size can also be seen (Figure 5e). Framboidal pyrite is about 35 μm in diameter, contains individually cubic or octahedral crystallites 0.1−2 μm in size, appears as strawberry-like aggregates, and the cementing materials in the framboids are fine-grained pyrite or kaolinite (Figure 5f). Siderite has a block and homogeneous

https://doi.org/10.1021/acsomega.3c00300
ACS Omega 2023, 8, 13884−13898

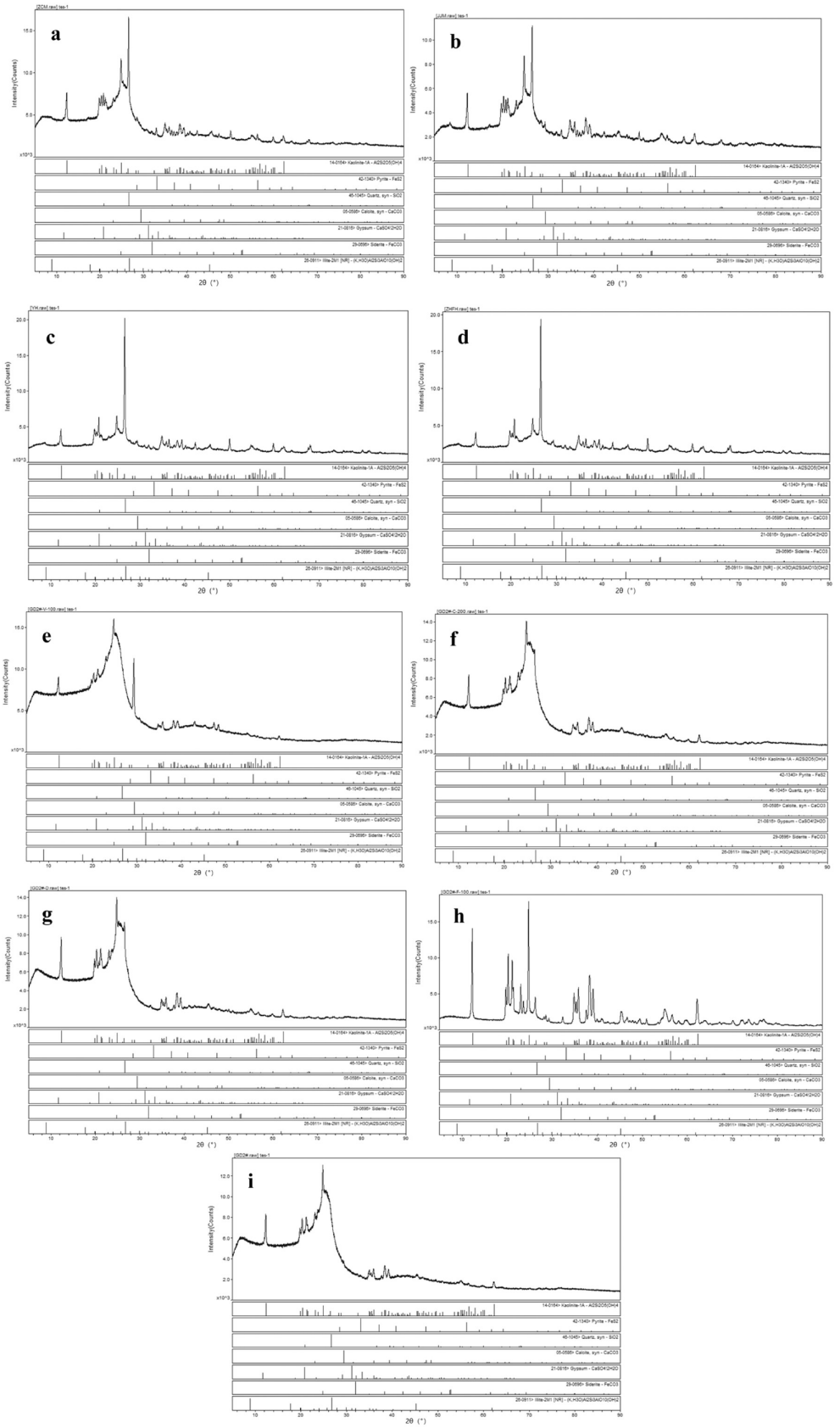

Figure 4. X-ray powder diffraction patterns of the coal dust and parent coal samples ((a) mining face, (b) heading face, (c) rocks roadway, (d) return airway, (e) vitrain, (f) clarain, (g) durain, (h) fusain, and (i) raw coal).

https://doi.org/10.1021/acsomega.3c00300
ACS Omega 2023, 8, 13884−13898

Table 3. Minerals in Underground Coal Dust and Parent Coal Samples (%)

sample		kaolinite	pyrite	quartz	calcite	gypsum	siderite	illite
coal dust	mining face	51.93	5.43	19.53	4.93	3.44	0.99	13.75
	heading face	38.92	2.35	10.00	1.58	7.25	15.26	24.63
	rock roadway	27.81	2.59	25.45	11.73	5.19	11.39	15.84
	return airway	34.29	2.42	23.85	6.29	9.86	14.46	8.84
parent coal	vitrain	43.02	1.66	3.29	21.81	22.27	6.52	1.43
	clarain	58.89	0.86	9.62	4.86	7.85	9.39	8.54
	durain	57.12	0.62	16.55	4.89	2.78	9.64	8.40
	fusain	52.46	1.18	5.85	4.27	11.76	19.35	5.13
	raw coal	74.44	0.40	5.36	8.12	2.74	0.41	8.54

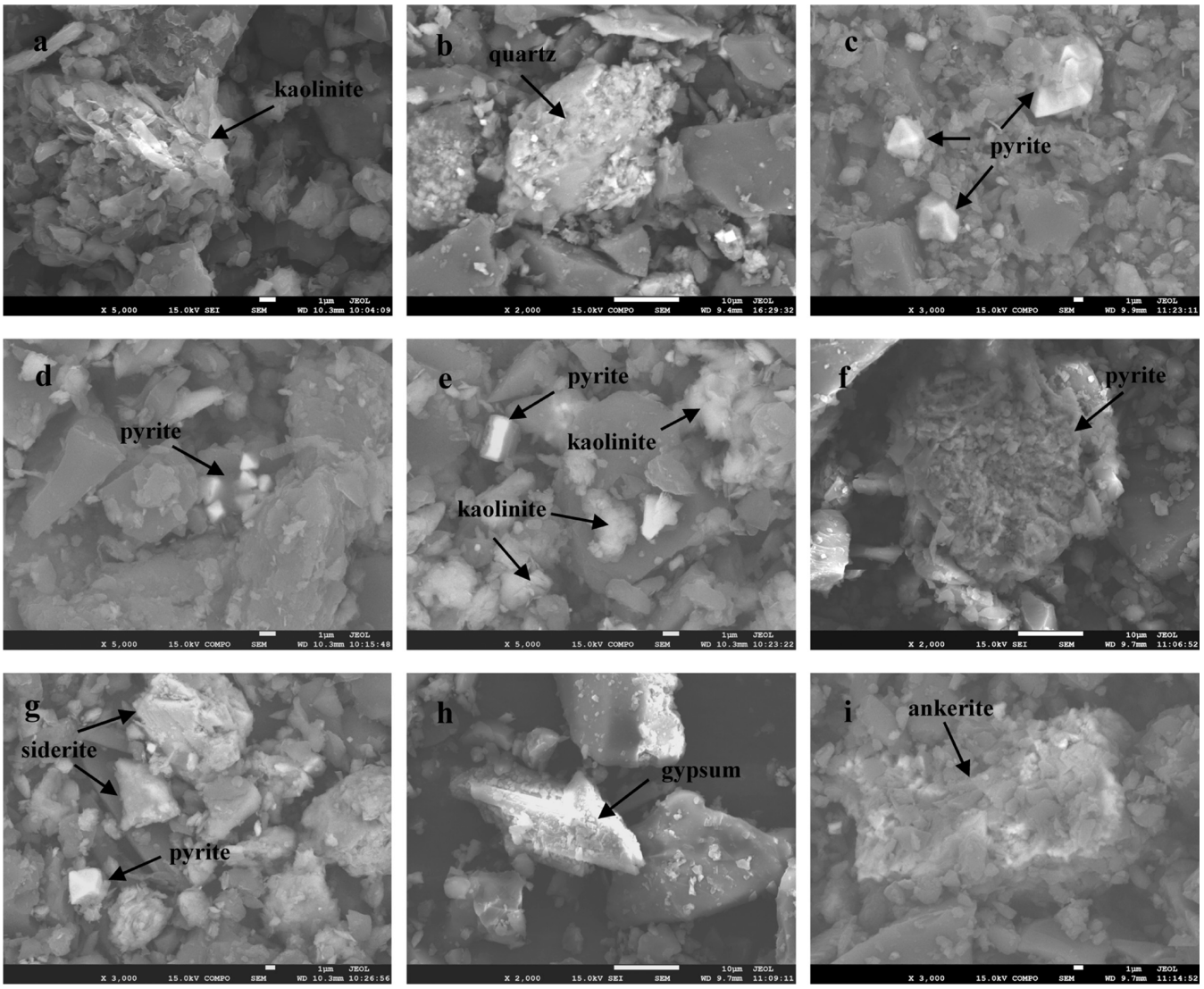

Figure 5. Scanning electron microscope images of the minerals in coal dust ((a) return airway, (b) mining face, (c) heading face, (d, e) return airway, (f) parent coal, (g) return airway, and (h, i) parent coal).

structure (Figure 5g), while gypsum has a plate-type structure (Figure 5h). Ankerite appears as fragmented lamellar aggregates (Figure 5i).

Besides, massive mineral aggregates contain anatase, kaolinite, and seldom siderite in the parent coal, along with Be, Cl, P, and S, which could be observed in many crystal lattices of minerals when they were enlarged (Figure S3a,b). The original HRTEM images were converted by the Fourier transform (FFT) image analysis method. The anatase (101) PDF (#75-1537) could be confirmed (Figure S3b). Nanocalcite (110) (PDF#05-0586) can be seen in the mining face coal dust, along with minor proportions of kaolinite, containing some trace elements, such as Mn, Sn, Sb, Be, and I (Figure 6a,b). The other three diffraction spots are (113), (012), and (006) (Figure 6b). Quartz with a relatively intact hexagonal columnar shape can be seen in the heading face sample, and some kaolinite in the crystal lattice in the heading face sample (Figure 6c−e). Nanomineral aggregates containing calcite,

https://doi.org/10.1021/acsomega.3c00300
ACS Omega 2023, 8, 13884−13898

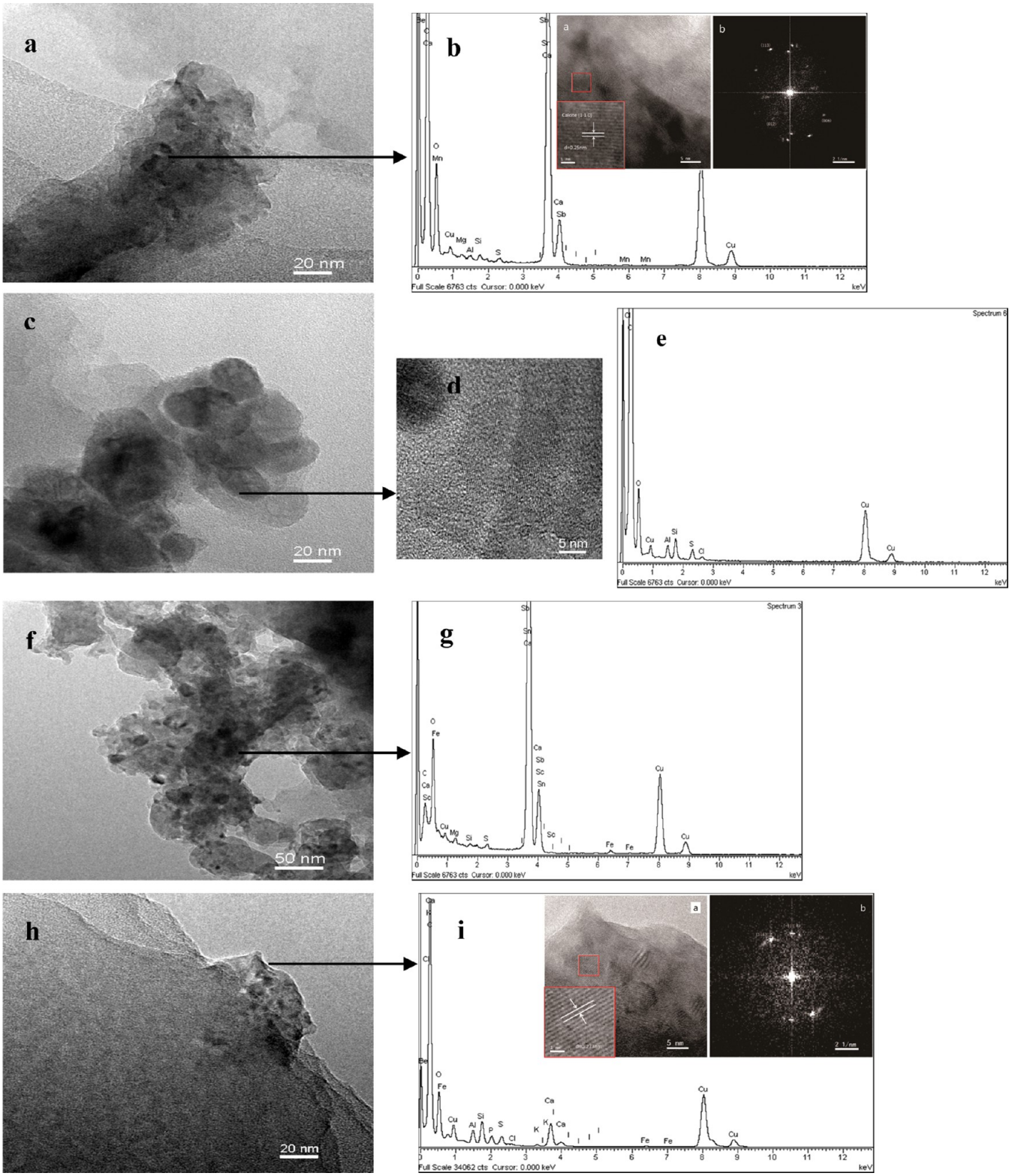

Figure 6. HRTEM-EDS images and analyzed results of minerals and trace elements in coal dust ((a, b) mining face, (c−e) heading face, (f, g) rocks roadway).

pyrite, iron dolomite, and abundant trace elements (Sc, Sb, Sn, and I) exist in the rocks roadway sample (Figure 6f,g). Massive spherical nanomineral aggregates containing siderite and seldom kaolinite can be observed, containing much Mn (Figure S3c,d). Spherical nanomineral aggregates containing calcite, siderite, and seldom kaolinite can be observed in Figure S3e, along with many quadrilateral sieve-shaped lattices and much Ti, V, and Nb in the rocks roadway coal dust (Figure S3f,g). The crystal planes at the three diffraction spots are (110), (012), and (104), and the crystal plane with a lattice spacing of 0.360 nm was siderite (012) (PDF#29-0696) (Figure 6h,i). The lattice spacing was 0.233 nm, which belongs

https://doi.org/10.1021/acsomega.3c00300
ACS Omega 2023, 8, 13884−13898

Table 4. Contents of As and Hg in the Coal Dust Samples, Lithotypes, and Raw Coal of Parent Coal, in Comparison with the Average Values for C−P Coal in North China (As in μg/g and Hg in ng/g)[a]

	underground coal dust				parent coal					AM	
element	mining face	heading face	rocks roadway	return airway	vitrain	clarain	durain	fusain	raw coal	NCC[47]	CC[17]
As	15.7	405	51.3	51.9	0.27	0.13	0.103	0.243	0.235	2.57	3.79
Hg	344	246	3894	3520	152	67.3	42.1	88.8	192	220	163

[a]NCC, C−P coal in North China; CC, Chinese coal; AM, arithmetic mean value.

Table 5. Modes of As and Hg Occurrence in Coal Dusts

element	sample	water-leachable	ion-exchangeable	carbonate-bound	silicate-bound	sulfide-bound	organic	total contents	extraction yields
As (μg/g)	mining face	0.01	0.18	0.19	3.2	11.48	0.02	15.08	0.96
	heading face	1.9	5.59	63.19	38.46	233.63	1.06	435.47	1.08
	rocks roadway	0.15	0.29	3.45	23.85	28.75	0.23	56.71	1.09
	return airway	0.07	0.21	2.1	7.99	41.27	0.09	51.73	1.01
Hg (ng/g)	mining face	<0.10	<0.10	67	18.25	162.75	81.2	329.2	0.957
	heading face	<0.10	<0.10	22.25	11.75	180.75	83.2	297.95	1.21
	rocks roadway	3	4.5	1662.5	280	1412.5	520	3882.5	1.1
	return airway	2.5	2.75	1275	272.5	1175	496	3223.75	0.828

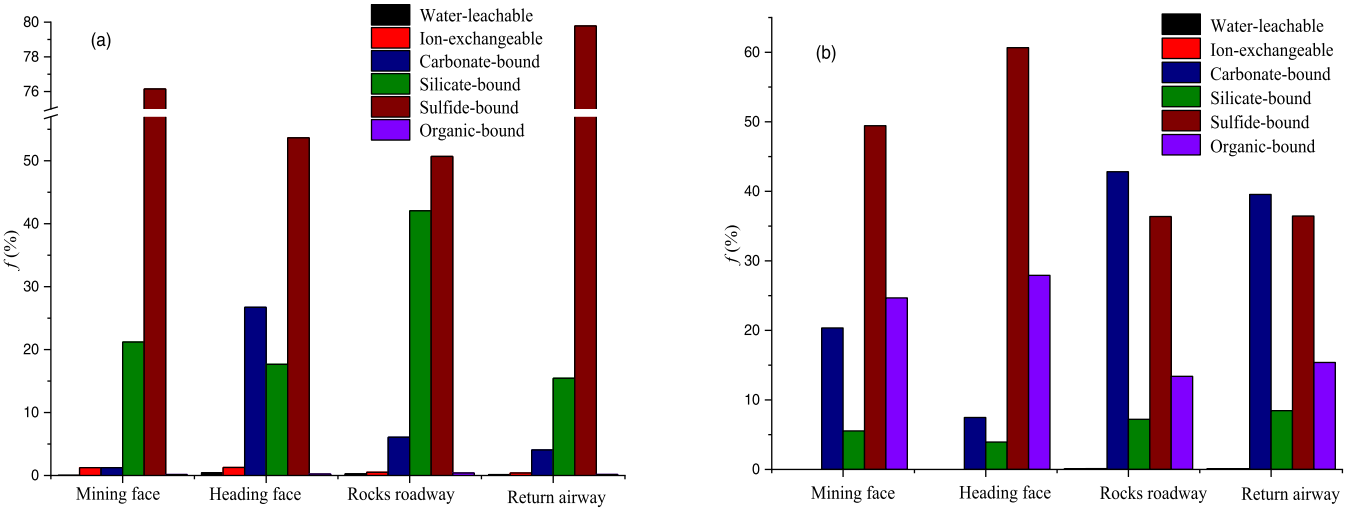

Figure 7. Percentage of extracted arsenic and mercury in each step for the underground coal dusts ((a) As, (b) Hg).

to nano-calcite (113) (PDF#05-0586) in Figure S3h,i. Nanomineral aggregates can be universally observed in the return airway sample, which are consistent with the XRD results.

3.3. Anomalous Concentrations of As and Hg in Coal Dust and Their Occurrence. *3.3.1. Contents of As and Hg in Coal Dust and No. 2 Parent Coal Samples.* The contents of As and Hg in the coal dust samples, lithotypes, and raw coal of parent coal, in comparison with the average values for C−P coal in North China[47] and Chinese Coal (CC),[17] are listed in Table 4. The results showed that the content of As ranges from 0.103 to 0.243 μg/g in the lithotypes, and is 0.235 μg/g in the raw coal. As is enriched in vitrain (0.27 μg/g) and fusain (0.243 μg/g). The concentration of As in the raw coal is much lower than that of the average for C−P coal in North China (2.57 μg/g), and it is also lower than the mean value in Chinese coal (3.79 μg/g). It can be found that As is abnormally concentrated in the coal dust samples. As is 15.7, 405, 51.3 and 51.9 μg/g in the mining face, heading face, rocks roadway, and return airway samples, respectively. The content of Hg ranges from 42.1 ng/g (durain) to 152 ng/g (vitrain) in the lithotypes, and Hg is relatively enriched in vitrain (152 ng/g) and fusain (88.8 ng/g). The concentration of Hg in the raw coal (192 ng/g) is normal in comparison with that of the average for C−P coal in North China (220 ng/g) and Chinese Coal (163 ng/g). Hg is 344, 246, 3894, and 3520 ng/g in the mining face, heading face, rocks roadway, and return airway samples, respectively.

The concentrations of As and Hg in the coal dust samples are greater than those in lithotypes and the raw coal of No. 2 parent coal. As contents in the coal dust samples are 66.81 (mining face), 1723.40 (heading face), 218.30 (rocks roadway), and 220.86 (return airway) times as high as the raw coal value, which is about one to three orders of magnitude above the parent coal value. Hg content in the mining face and heading face samples is normal compared to the concentration in raw coal, while the Hg contents in the rocks roadway and return airway samples are 20.28 and 18.33 times as high as the raw coal value, respectively. Based on the enrichment classification, the concentrations of trace elements in coal can be classified into six categories, unusually enriched (E_f > 100), significantly enriched (10 < E_f < 100), enriched (5 < E_f <

https://doi.org/10.1021/acsomega.3c00300
ACS Omega 2023, 8, 13884−13898

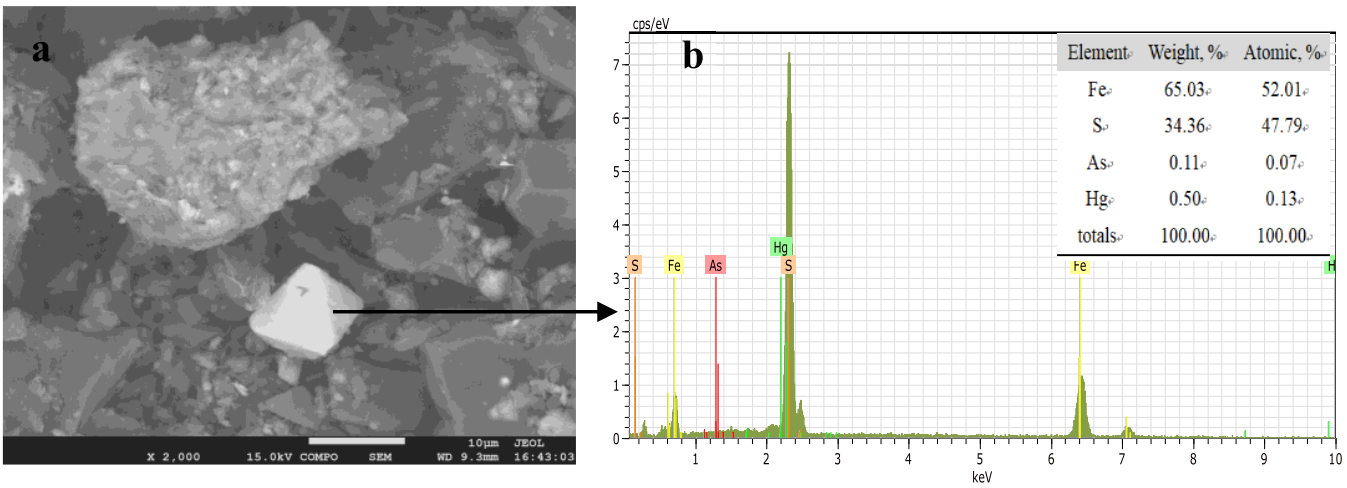

Figure 8. FESEM-EDS image of octahedral pyrite crystal (diameter near 10 μm) with As (wt %, 0.11) and Hg (wt %, 0.50); kaolinite containing quartz aggregates (mining face sample) ((a) FESEM image, (b) EDS spectrum and its result).

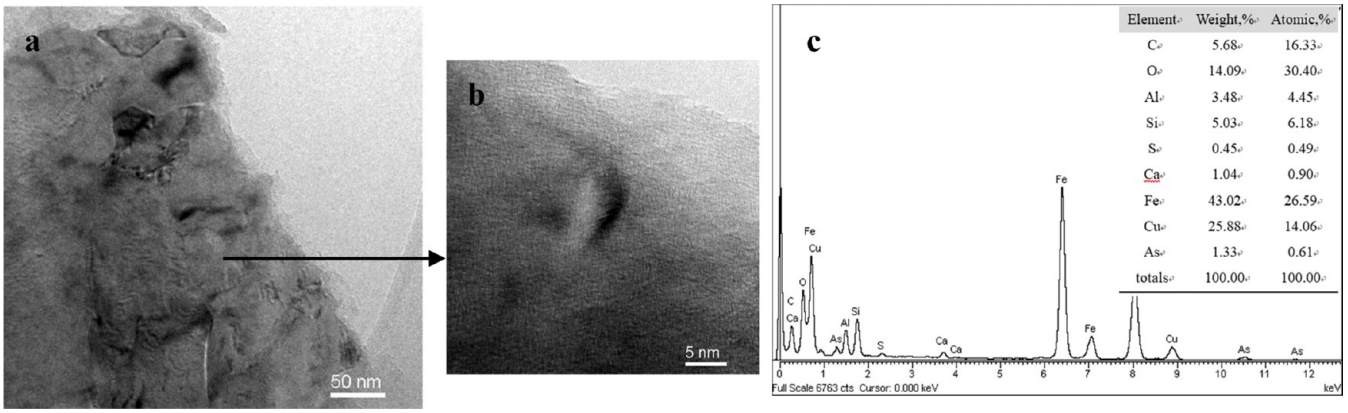

Figure 9. (a) HRTEM-EDS images of particles containing siderite, calcite, kaolinite, and pyrite, along with much As (wt %, 1.33) (heading face sample). The Cu peak is related to the Cu grid; (b) HRTEM enlarged image exhibiting many lattice fringes of minerals and organic matters; (c) EDS spectrum and its result.

10), slightly enriched ($2 < E_f < 5$), normal ($0.5 < E_f < 2$), and depleted ($E_f < 0.5$).[17] It can be concluded that As is unusually enriched in the coal dust samples, while Hg is normal in the mining face and heading face samples, and significantly enriched in the rocks roadway and return airway samples.

3.3.2. Modes of Occurrence of As and Hg in Coal Dust. The modes of As and Hg occurrence were determined by sequential chemical extraction, which were identified into six types, i.e., water-soluble, ion-exchange, carbonate-bound, silicate-bound, disulfide-bound, and organic-bound. The results are listed in Table 5. It was found that the total contents of As are 15.08, 435.47, 56.71, and 51.73 μg/g, and Hg are 329.2, 297.95, 3882.5, and 3223.75 ng/g in mining face, heading face, rocks roadway, and return airway samples, respectively. In comparison with the total As contents directly determined by AFS, the extraction yields are 95.7%, 1.21, 1.10, and 82.8, and in comparison with the total Hg contents determined by the mercury director, the extraction yields are 95.7%, 1.21, 1.10, and 82.8%, respectively.

The As occurrence is mainly disulfide-bound in the coal dust samples, accounting for 76.15, 53.65, 50.69, and 79.78%, respectively; carbonate-bound and silicate-bound As were the secondarily abundant forms in the heading face coal dust, accounting for 26.72 and 17.66%, respectively; silicate-bound was the secondarily abundant As form in mining face, rocks roadway, and return airway samples. A minor content of water-soluble and organic-bound As host was found in the coal dust samples (Figure 7a). Disulfide-bound Hg dominated in mining face and heading face samples; the contents were 162.75 and 180.75 ng/g, accounting for 49.44 and 60.66%, respectively; organic-bound Hg was the secondarily abundant form, and the contents were 81.2 and 83.2 ng/g, accounting for 24.67 and 27.92%, respectively. The modes of Hg occurrence are dominated by carbonate-bound and disulfide-bound in rocks roadway and return airway samples. The contents of carbonate-bound and disulfide-bound Hg are 1662.5 and 1412.5 ng/g in the rocks roadway sample, accounting for 42.82 and 36.38%, respectively; the contents are 1275 and 1175 ng/g in the return airway sample, accounting for 39.55 and 36.45%, respectively (Figure 7b).

The SEM image of octahedral pyrite crystal (diameter near 10 μm) with the EDS spectra showing As (wt %, 0.11) and Hg (wt %, 0.50) can be observed in the mining face sample (Figure 8). HRTEM-EDS was applied to demonstrate the trace element occurrence and to determine the nanominerals. Figure 9a illustrates the HRTEM image of nanoparticles in the coal dust of heading face containing siderite, calcite, kaolinite, and pyrite, with the occurrence of As (wt %, 1.33). It exhibits many

https://doi.org/10.1021/acsomega.3c00300
ACS Omega 2023, 8, 13884−13898

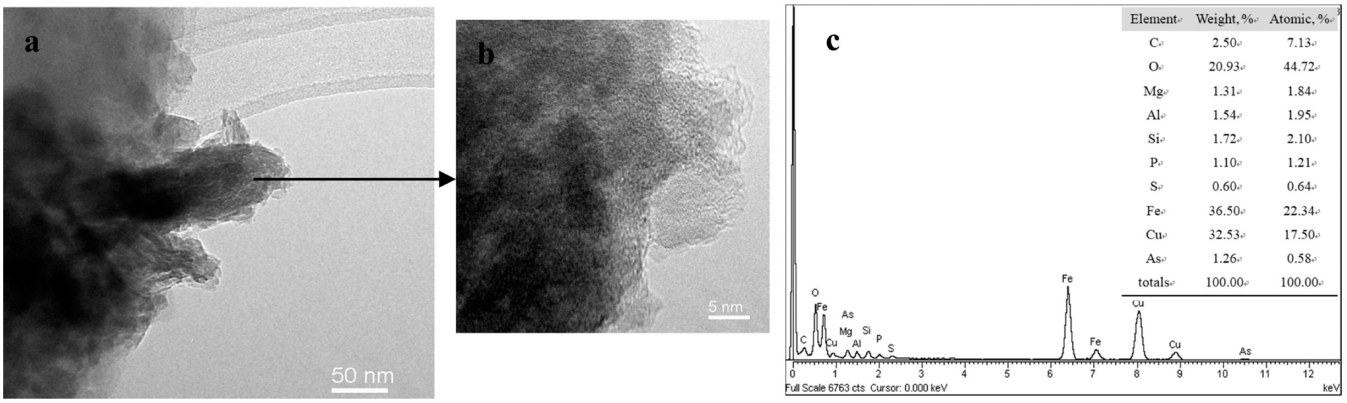

Figure 10. HRTEM-EDS images of coal dust containing aromatic microcrystals, minerals (darker areas) (such as kaolinite, siderite, magnesite, and pyrite), along with much As (wt %, 1.26) (heading face sample) ((a) HRTEM image of nanoparticles, (b) HRTEM enlarged image, (c) EDS spectrum and its result).

Table 6. Contents of Hazardous Trace Elements in Coal Dust and Parent Coal, and Comparison with the Average Values for C−P Coal in North China and Chinese Coal (μg/g, Hg in ng/g)[a]

element	mining face	heading face	rocks roadway	return airway	vitrain	clarain	durain	fusain	raw coal	NCC[47]	CC[17]
As	15.7	405	51.3	51.9	0.27	0.13	0.103	0.243	0.235	2.57	3.79
Cd	0.19	1.25	0.643	0.558	0.062	0.029	0.041	0.087	0.037	0.30	0.25
Cr	16.1	17.3	32.2	34.7	8.96	16	19.4	33.8	40.3	15.81	15.4
Hg	344	246	3894	3520	152	67.3	42.1	88.8	192	220	163
Se	1.27	2.19	1.84	1.79	1.8	0.416	0.566	0.164	0.063	4.84	2.47
Cl	1770	11200	4620	4790	2180	1440	1140	640	1620	389	255
F	210	300	140	260	1560	470	1040	509	498	148.4	130
Mn	80.1	98	166	161	40.8	11.1	13.3	13.3	22	56.8	125
Mo	2.83	2.57	2.55	2.6	0.332	0.186	0.199	0.898	0.273	3.47	3.08
Ni	8.18	8.38	12.8	14.7	2.67	1.3	1.43	11.9	1.4	11.75	13.7
Pb	17.6	116	62.9	58.4	4.1	2.34	2.32	15.7	2.88	20.34	15.1
Be	1.63	1.32	2.24	2.08	0.424	0.635	0.558	1.56	0.434	1.92	2.11
Cu	10.5	21.1	27.4	31.1	7.72	12.1	13.8	3.38	11.5	21.97	17.5
Th	6.99	10.8	10.4	11.2	4.82	10.8	6.99	5.41	4.68	8.71	5.84
U	2.65	2.6	2.68	2.78	0.846	2.6	2.65	4.92	0.961	2.60	2.43
V	27.9	27.6	50.1	53.4	13.1	11.1	10.6	158	198	39.59	35.1
Zn	32.6	41	87.6	106	49.1	18.1	16.5	22.5	34.5	48.99	41.4
Ba	154	157	309	323	32.6	33.3	37.7	54.1	32.9	121.59[17]	159
Co	3.13	2.98	7.48	7.77	0.909	0.389	0.251	0.782	0.473	4.24	7.08
Sb	4	24.7	12.6	12.4	0.206	0.09	0.085	0.206	0.14	0.68	0.84
Tl	0.533	0.25	0.404	0.423	0.038	0.02	0.024	0.035	0.037	0.35	0.47

[a]NCC, C−P coal in North China; CC, Chinese coal; AM, standard arithmetic mean value.

lattice fringes when the dot is enlarged (Figure 9b). The HRTEM images contained aromatic lattice fringes, minerals (darker areas) (such as kaolinite, siderite, magnesite, and pyrite), along with much As in the heading face sample (wt %, 1.26) (Figure 10). The HRTEM-EDS observation is consistent with the high concentration of As (405 μg/g) in the heading face sample measured by AFS.

3.4. Enrichment Mechanism of As and Hg in Coal Dust. The former results suggested that large amounts of As and Hg could be contained in some airborne grains and possibly derived from their formation process. The low concentrations of As and Hg in coal make the enrichment mechanism of coal dust more complex. In a comparison of harmful trace elements in coal dust samples with lithotypes of parent coal (Table 6 and Figure 11a−d), it was found that As, Hg, Pb, and Sb were concentrated in all coal dusts: especially As (405 μg/g) in the heading face sample, Pb (116 μg/g) in the heading face sample, and Hg, Pb in rocks roadway and return airway coal dusts. The concentrations of some harmful trace elements in the coal dust samples investigated vs No. 2 parent coal are as follows: As (66.81,1723.40, 218.30, and 220.85), Cd (5.14, 33.78, 17.38, and 15.08), Hg (1.79, 1.28, 20.28, and 18.33), Se (20.16, 34.76, 29.21, and 28.41), Mo (10.37, 9.41, 9.34, and 9.52), Ni (5.84, 5.99, 9.14, and 10.5), Pb (6.11, 40.28, 21.84, and 20.28), Co (6.62, 6.30, 15.81, and 16.43), Sb (28.57, 176.43, 90, and 88.57), and Tl (14.41, 6.76, 10.92, and 11.43) for mining face, heading face, rocks roadway, and return airway, respectively. The contents of As, Cd, Hg, Se, Mo, Ni, Pb, Co, Sb, and Tl in mining face, heading face, rocks roadway, and return airway samples are many times higher than those of the parent coal. Coal dust particles with fine size and large surface area have strong adsorption capacity and are the main carriers of volatile elements and nanominerals. During coal mining, the elements, especially As, Cd, Hg, Se, Pb, Co, Sb, and Tl, are released or are present in the

https://doi.org/10.1021/acsomega.3c00300
ACS Omega 2023, 8, 13884−13898

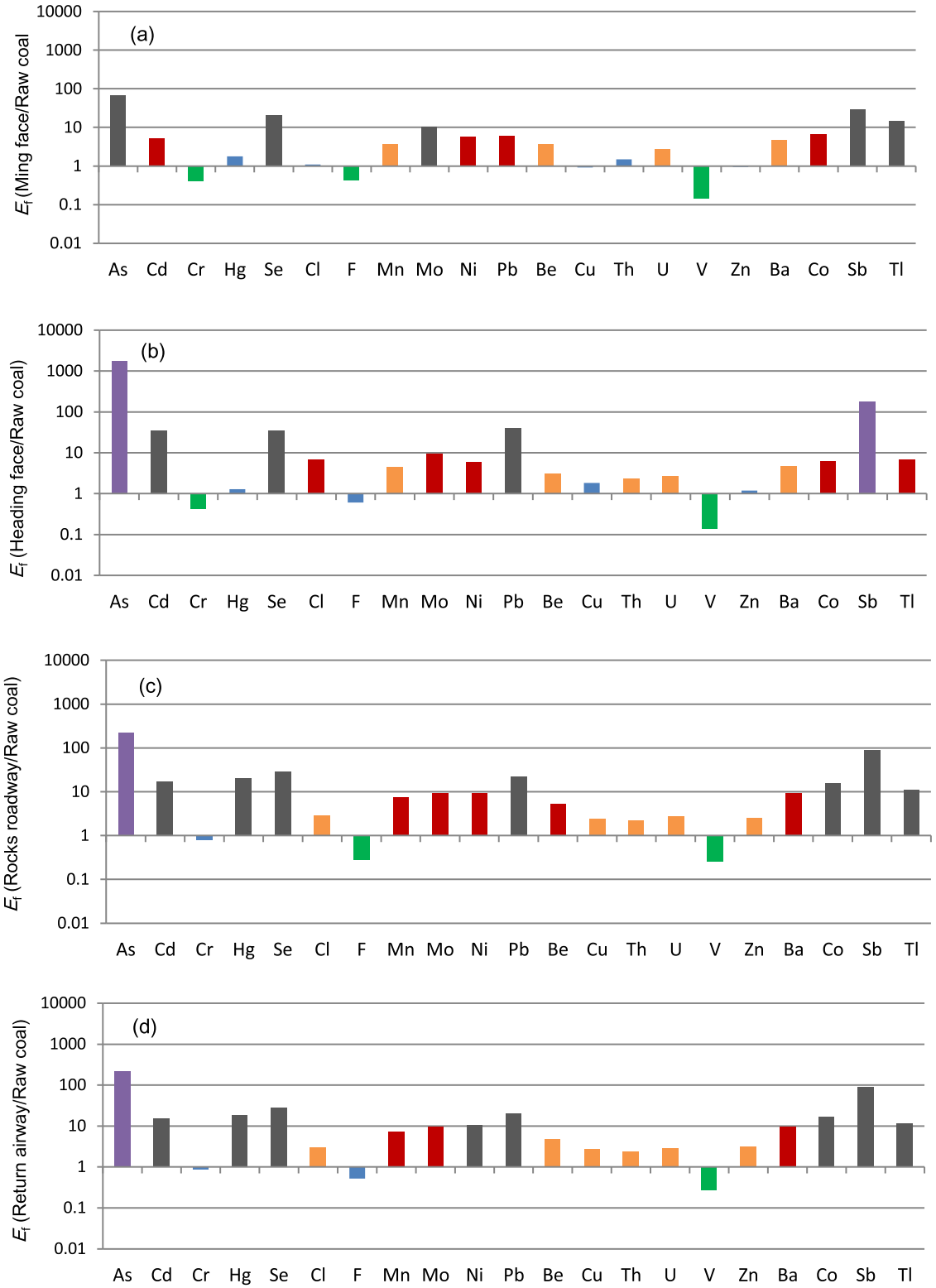

Figure 11. Comparison of the contents of harmful trace elements in the coal dust with the No. 2 parent coal (E_f > 100 (purple): unusually enriched; 10 < E_f < 100 (black): significantly enriched; 5 < E_f < 10 (red): enriched; 2 < E_f < 5 (orange): slightly enriched; 0.5 < E_f < 2 (blue): normal; E_f < 0.5 (green): depleted) ((a) mining face, (b) heading face, (c) rocks roadway, (d) return airway).

nanominerals, which can easily be concentrated in the underground airborne dusts.

The formation of underground coal dust undergoes a strongly mechanical crushing process, which will lead to the mechanochemical function. In comparison with the parent coal, the chemical structure, surface properties, and pore structures of coal dust were modified: the bridge bonds and cross-link bonds in coal macromolecular structure were broken; staged and unsaturated structures on the surface were formed; the porosity and crack structures were

https://doi.org/10.1021/acsomega.3c00300
ACS Omega 2023, 8, 13884−13898

changed.[48] The mechanochemical effect not only leads to coal particles being refined and the specific surface area being increased, but can also result in lattice distortion, lattice defects (such as suspended bonds), formation of free radicals, increase of surface free energy, appearance of plasma state, etc.[49] The X-ray diffraction line profile analysis indicated that no pyrite phase transformation occurred, but the crystallite size decreased, and microstrain increased during the mechanical activation process.[50] In comparison with parent coal, the structure and morphology modification of airborne particulates will have a significant influence on the absorption ability of miner grains and volatile elements. The FESEM-EDS and HRTEM-EDS observations of the coal fly ash particles with 0.1−100 nm size demonstrate that the materials contain a small proportion of encapsulated hazardous volatile elements (HVEs), such as As, Hg, Pb, Se, and nanoparticles with multiple nanomineral assemblages.[51,52] There is a strong positive correlation between the Hg concentration and the BET/Langmuir specific surface area, mesopore volume, and micropore surface area.[52] The detrital and vegetal minerals, and their evolution, are the basic origins of As and Hg; the particle morphology and structure modifications enhance the adsorption abilities of miner particulates containing nanominerals and volatile elements, which is the dominant factor. In summary, the possible formation processes of anomalous concentrations of As and Hg in coal dust are shown in Figure 12.

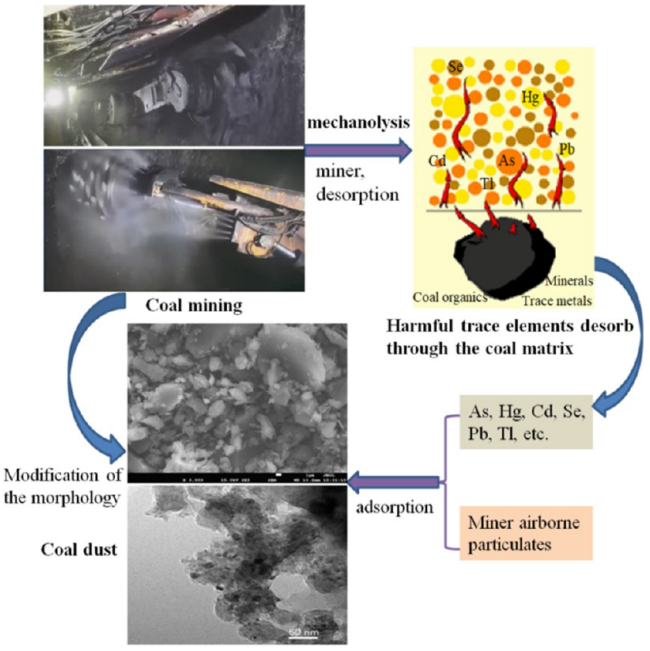

Figure 12. Possible formation processes of anomalous concentrations of As and Hg in underground coal dust.

4. CONCLUSIONS

The investigation of coal dust particle size distribution, mineralogical, and geochemical characteristics is the basis for dust control and prevention of occupational diseases. In this paper, the coal dust directly collected from the mining faces, heading face, rocks roadway, and return air roadway of No. 2 coal seam, Xishan coalfield, Shanxi province, North China was systematically investigated. The main conclusions are as follows.

(1) Laser particle size analysis indicated that $PM_{2.5}$ accounted for 4.09, 7.62, 9.94, and 9.12%, and PM_5 accounted for 10.09, 15.71, 24.58, and 21.69%. In comparison with manual coal dust, underground coal dusts capture many fine particulates on the surface, and have more pyrite and quartz. The minerals in the coal dust samples are mainly dominated by kaolinite, quartz, illite, siderite, gypsum, calcite, and pyrite, with minor amounts of barite and ankerite, which are observed by XRD, SEM, and HRTEM in conjunction with EDS analysis.

(2) As and Hg are enriched in vitrain and fusain, and the contents of As and Hg were depleted or normal in the parent coal samples compared with the average values of C−P coal in North China and Chinese coal. As and Hg are anomalously enriched in the coal dust samples studied. The arsenic content in mining face, heading face, rocks tunnel, and return airway samples is 15.7, 405, 51.3, and 51.9 μg/g, while mercury content is 344, 246, 3894, and 3520 ng/g, respectively. The concentrations of As and Hg in the coal dust samples studied are greater than the values of these elements in No. 2 parent coal. The As content in the coal dust samples studied is about one to three orders of magnitude above the parent coal value and Hg content in the studied coal is 1.28 to 20.28 times as high as the parent coal value.

(3) Sequential extraction procedures were performed to study the possible modes of occurrence of As and Hg in coal dust samples. The occurrence of As is dominated mainly by pyrite and secondarily by carbonate and silicate in the coal dust samples. The pyritic Hg and organic Hg may be the dominant forms in mining face and heading face samples, and carbonate and pyritic Hg are the main forms in rocks roadway and return airway samples.

(4) It is considered that mechanochemical effect results in the formation of surface active sites and modification of the morphology. Volatile elements and miner grains, which are associated with nanominerals bearing much hazardous elements, could easily be originally fractionated or adsorbed by airborne particulates. This research aims to provide a theoretical basis for prevention of occupational disease and underground environmental evaluation.

■ ASSOCIATED CONTENT

Supporting Information

The Supporting Information is available free of charge at https://pubs.acs.org/doi/10.1021/acsomega.3c00300.

SEM-EDS images of minerals in coal dust (Figure S1); SEM images of organic matters and minerals in coal dust (secondary electron mode and backscattered electron mode) (Figure S2); HRTEM-EDS images and analyzed results of minerals and trace elements in coal dust (Figure S3) (PDF)

■ AUTHOR INFORMATION

Corresponding Author

Chuange Wang − *Department of Earth Science and Engineering, Taiyuan University of Technology, Taiyuan*

https://doi.org/10.1021/acsomega.3c00300
ACS Omega 2023, 8, 13884−13898

030024, China; Shanxi Key Laboratory of Coal and Coal-measure Gas Geology, Taiyuan 030024, China;
orcid.org/0000-0002-9961-156X;
Email: wangchuange@tyut.edu.cn

Authors

Fangui Zeng − *Department of Earth Science and Engineering, Taiyuan University of Technology, Taiyuan 030024, China; Shanxi Key Laboratory of Coal and Coal-measure Gas Geology, Taiyuan 030024, China*

Chengxiang Xu − *Department of Earth Science and Engineering, Taiyuan University of Technology, Taiyuan 030024, China; Shanxi Key Laboratory of Coal and Coal-measure Gas Geology, Taiyuan 030024, China*

Qiuyue Xu − *Department of Earth Science and Engineering, Taiyuan University of Technology, Taiyuan 030024, China; Shanxi Key Laboratory of Coal and Coal-measure Gas Geology, Taiyuan 030024, China*

Complete contact information is available at:
https://pubs.acs.org/10.1021/acsomega.3c00300

Notes

The authors declare no competing financial interest.

■ ACKNOWLEDGMENTS

This work was financially supported by the Fundamental Research Program of Shanxi Province (20210302123137), the National Natural Science Foundation of China (41973077), and the NSFC-Shanxi Coal-based low Carbon joint Fund (U1510102). The contents of As, Hg, and major elements in coal dust were analyzed at the Analytical Laboratory of Beijing Research Institute of Uranium Geology (BRIUG). The authors thank the Analytical Laboratory of BRIUG staff for the technical support.

■ REFERENCES

(1) Yucesoy, B.; Luster, M. I. Genetic susceptibility in pneumoconiosis. *Toxicol. Lett.* **2007**, *168*, 249−254.
(2) Fishwick, D.; Barber, C. Pneumoconiosis. Syst. *Parench. lung dis.* **2012**, *40*, 310−313.
(3) Perret, J. L.; Plush, B.; Lachapelle, P.; et al. Coal mine dust lung disease in the modern era. *Respirology* **2017**, *22*, 662−670.
(4) Liu, T.; Liu, S. M. The impacts of coal dust on miners' health: A review. *Environ. Res.* **2020**, *190*, No. 109849.
(5) Riley, K. W.; French, D. H.; Farrell, O. P.; Wood, R. A.; Huggins, F. E. Modes of occurrence of trace and minor elements in some Australian coals. *Int. J. Coal Geol.* **2012**, *94*, 214−224.
(6) Harrison, J. C.; Brower, P. S.; Attfield, M. D.; Doak, C. B.; Keane, M. J.; Grayson, R. L.; Wallace, W. E. Surface composition of respirable silica particles in a set of U.S. anthracite and bituminous coal mine dusts. *J. Aerosol Sci.* **1997**, *28*, 689−696.
(7) Ding, M.; Chen, F.; Shi, X. L.; Yucesoy, B.; Mossman, B.; Vallyathan, V. Diseases caused by silica: mechanisms of injury and disease development. *Int. Immunopharmacol.* **2002**, *2*, 173−182.
(8) Castranova, V. Signaling pathways controlling the production of inflammatory mediators in response to crystalline silica exposure: role of reactive oxygen/nitrogen species. *Free Radical Biol. Med.* **2004**, *37*, 916−925.
(9) Serol, I.; Aydin, H.; Didari, V.; Ural, S. Pneumoconiosis and quartz content of respirable dusts in the coal mines in Zonguldak, Turkey. *Int. J. Coal Geol.* **2013**, *116*−*117*, 26−35.
(10) Harrington, A. D.; Tsirka, S. E.; Schoonen, M. A. A. Inflammatory stress response in A549 cells as a result of exposure to coal: Evidence for the role of pyrite in coal workers' pneumoconiosis pathogenesis. *Chemosphere* **2013**, *93*, 1216−1221.
(11) Stone, V.; Jones, R.; Rollo, K.; Duffin, R.; Donaldson, K.; Brown, D. M. Effect of coal mine dust and clay extracts on the biological activity of the quartz surface. *Toxicol. Lett.* **2004**, *149*, 255−259.
(12) Schulz, H. M. Coal mine workers' pneumoconiosis-Application of coal petrographical and organic geochemical methods carried out on coals, coal mine dust, and isolated lung dust. *Environ. Geol.* **1997**, *30*, 72−80.
(13) Sarver, E.; Keles, C.; Rezaee, M. Characteristics of respirable dust in eight appalachian coal mines: A dataset including particle size and mineralogy distributions, and metal and trace element mass concentrations. *Data Brief* **2019**, *25*, No. 104032.
(14) Sarver, E.; Keles, C.; Rezaee, M. Beyond conventional metrics: comprehensive characterization of respirable coal mine dust. *Int. J. Coal Geol.* **2019**, *207*, 84−95.
(15) Su, X. B.; Ding, R.; Zhuang, X. G. Characteristics of Dust in Coal Mines in Central North China and Its Research Significance. *ACS Omega* **2020**, *5*, 9233−9250.
(16) Trechera, P.; Moreno, T.; Cordoba, P.; Moreno, N.; Zhuang, X. G.; Li, B. Q.; Li, J.; Shangguan, Y. F.; Kandler, K.; Dominguez, A. O.; Kelly, F.; Querol, X. Mineralogy, geochemistry and toxicity of size-segregated respirable deposited dust in underground coal mines. *J. Hazard. Mater.* **2020**, *399*, No. 122935.
(17) Dai, S. F.; Ren, D. Y.; Chou, C. L.; Finkelman, R. B.; Seredin, V. V.; Zhou, Y. P. Geochemistry of trace elements in Chinese coals: a review of abundances, genetic types, impacts on human health, and industrial utilization. *Int. J. Coal Geol.* **2012**, *94*, 3−21.
(18) Goodarzi, F.; Swaine, D. J. *Environmental Aspects of Trace Elements in Coal*; Kluwer Acad. Publishers: Dordrecht, 1995; p 312.
(19) Finkelman, R. B. Trace elements in coal: Evironmental and health significance. *Biol. Trace Elem. Res.* **1999**, *67*, 197−204.
(20) Ren, D. Y.; Zhao, F. H.; Zhang, J. Y.; Xu, D. W. A preliminary study on genetic type of enrichment for hazardous minor and trace elements in coal. *Earth Sci. Front.* **1999**, *6*, 17−22.
(21) Zhao, F. H.; Ren, D. Y.; Yin, J. S.; Li, Y. N.; Wang, X. Q. The Study on the occurrence of arsenic in coal by sequential chemical extract. *Environ. Sci.* **1999**, *20*, 79−81.
(22) Ding, Z. H.; Zheng, B. S.; Finkelmam, R. B.; Belkin, H. E.; Hu, T. D.; Liu, T. Application of XAFS and Mö ssbauer spectroscopy in studying the mode of occurrence of arsenic and iron in high-As coals from Southwest Guizhou Province. *Geol. J. China Univ.* **2003**, *9*, 273−278.
(23) Liu, G. J.; Zheng, L. G.; Zhang, Y. Distribution and mode of occurrence of As, Hg, Se and sulfur in coal seam 3 of the Shanxi Formation, Yanzhou Coalfield, China. *Int. J. Coal Geol.* **2007**, *71*, 371−385.
(24) Huang, W. H.; Yang, Y. C. Mercury in Coal of China. *Coal Geol. China* **2002**, *14*, 37−40.
(25) Zheng, L. G.; Liu, G. J.; Qi, C. C.; Zhang, Y.; Wong, M. H. The use of sequential extraction to determine the distribution and modes of occurrence of mercury in Permian Huaibei coal, Anhui Province, China. *Int. J. Coal Geol.* **2008**, *73*, 139−155.
(26) Kolker, A.; Huggins, F. E.; Palmer, C. A.; Shah, N.; Crowley, S. S.; Huffman, G. P.; Finkelman, R. B. Mode of occurrence of arsenic in four US coals. *Fuel Process. Technol.* **2000**, *63*, 167−178.
(27) Yudovich, Y. E.; Ketris, M. P. Arsenic in coal: a review. *Int. J. Coal Geol.* **2005**, *61*, 141−196.
(28) Yudovich, Y. E.; Ketris, M. P. Mercury in coal: a review Part 1. Geochemistry. *Int. J. Coal Geol.* **2005**, *62*, 107−134.
(29) Finkelman, R. B.; Palmer, C. A.; Wang, P. P. Quantification of the modes of occurrence of 42 elements in coal. *Int. J. Coal Geol.* **2018**, *185*, 138−160.
(30) Palmer, C. A.; Krasnow, M. R.; Finkelman, R. B. An evaluation of leaching to determine modes of occurrence of selected toxic elements in coal. *J. Coal Qual.* **1993**, *12*, 135−141.
(31) Maciejewska, A. Occupational exposure assessment for crystalline silica dust: approach in Poland and worldwide. *Environ. Health* **2008**, *21*, 1−23.

(32) Moreno, T.; Trechera, P.; Querol, X.; Lah, R.; Johnson, D.; Wrana, A.; Williamson, B. Trace element fractionation between PM10 and PM2.5 in coal mine dust: implications for occupational respiratory health. *Int. J. Coal Geol.* **2019**, *203*, 52−59.
(33) GB/T 6948-2008 (National Standard of P. R. China) Method of determining microscopically the reflectance of vitrinite in coal (in Chinese), 2008.
(34) GB/T 212-2008 (National Standard of P. R.) China Proximate analysis of coal (in Chinese), 2008.
(35) GB/T 476-2008 (National Standard of P. R. China) Determination of carbon and hydrogen in coal (in Chinese), 2008.
(36) GB/T 214-2007 (National Standard of P. R. China) Determination of total sulfur in coal (in Chinese), 2007.
(37) Zhao, Y. Y.; Liang, H. Z.; Zeng, F. G.; Tang, Y. G.; Liang, L. T.; Takahashi, F. Origins and occurrences of Ti-nanominerals in a superhigh-organic-sulfur coal. *Fuel* **2020**, *259*, No. 116302.
(38) GB/T 14506.28-2010 (National Standard of P. R. China) Chemical analysis of silicate rocks Part 28: Measurement of 16 principal and secondary components (in Chinese), 2010.
(39) GB/T 14506.12-2010 (National Standard of P.R. China) Chemical Analysis of Silicate Rocks Part 12: Fluorine measurement (in Chinese), 2010.
(40) GB/T 14506.30-2010 (National Standard of P.R. China) Chemical Analysis of Silicate Rocks Part 30: Determination of 44 elements (in Chinese), 2010.
(41) GB/T 22105.2-2008 (National Standard of P. R. China) Determination of total mercury, arsenic and lead in soil quality Part 2: Determination of total arsenic in soil (in Chinese), 2008.
(42) EJ/T 1149-2001 (National Standard of P.R. China) Determination of trace bismuth and mercury in uranium-bearing ores by hydride generation-double channel atomic fluorescence spectrometry (in Chinese), 2001.
(43) DZ/T 0064.11-1993 (National Standard of P.R. China) Groundwater quality inspection method for the determination of arsenic by gas-liquid separation hydride atomic fluorescence spectrometry (in Chinese), 1993.
(44) EPA 7473-2007 (US) Thermal decomposition dydride atomic absorption spectrometry for the determination of mercury in solids and liquids, 2007.
(45) Zhao, Y. F. *Mine Dust Prevention and Control Technology*; Coal Industry Press: Beijing, 2007; p 2.
(46) Cang, E. Z.; Liu, S. C. Study on the harm of coal dust to respiratory system. *Ind. Health Occup. Dis.* **1989**, *15*, 265−268.
(47) Ren, D. Y.; Zhao, F. H.; Dai, S. F.; Zhang, J. Y.; Ge, K. L. *Geochemistry of Trace Elements in Coal*; Science Press: Beijing, 2006; pp 82−83.
(48) Yang, J. *Study on Wetting Mechanism of Coal Dust*; Shandong University Science of Technology, 2010.
(49) Zhang, L. X.; Li, G. C. Research progress of mechanochemistry effect of mineral ultrafine grinding. *Exp. Inf. Min. Ind.* **2007**, *6*, 31−34.
(50) Pourghahramani, P.; Akhgar, B. N. Characterization of structural changes of mechanically activated natural pyrite using XRD line profile analysis. *Int. J. Miner. Process.* **2015**, *134*, 23−28.
(51) Ribeiro, J.; DaBoit, K.; Flores, D.; Kronbauer, M. A.; Silva, L. F. O. Extensive FE-SEM/EDS, HR-TEM/EDS and ToF-SIMS studies of micron- to nano-particles in anthracite fly ash. *Sci. Total Environ.* **2013**, *452−453*, 98−107.
(52) Kostova, I.; Vassileva, C.; Dai, S. F.; Hower, J. C.; Apostolova, D. Influence of surface area properties on mercury capture behaviour of coal fly ashes from some Bulgarian power plants. *Int. J. Coal Geol.* **2013**, *116−117*, 227−235.

https://doi.org/10.1021/acsomega.3c00300
ACS Omega 2023, 8, 13884−13898